Journal of Cystic Fibrosis xxx (xxxx) xxx

Contents lists available at ScienceDirect

Journal of Cystic Fibrosis

journal homepage: www.elsevier.com/locate/jcf

Original Article

Transcriptomic and functional profiling of human intestinal organoids identifies enhanced calcium signalling and thrombospondin-2 activity in cystic fibrosis

Ellie Slater [a,1], Woo Jin Yang [a,c,1], Nefeli Skoufou-Papoutsaki [b], Stephen A. Renshaw [d], Róisín M. Owens [c], Matthias Zilbauer [a,*]

[a] Cambridge Stem Cell Institute, University of Cambridge, Cambridge, UK
[b] Cancer Research UK Cambridge Institute, University of Cambridge, Cambridge, UK
[c] Department of Chemical Engineering and Biotechnology, University of Cambridge, Cambridge, UK
[d] Bateson Centre and School of Medicine and Population Health, University of Sheffield, Sheffield, UK

ARTICLE INFO

Keywords:
Human intestinal organoids
Cystic fibrosis
CRISPR
Calcium dysregulation
CFTR

ABSTRACT

Background: Although gastrointestinal symptoms of cystic fibrosis (CF) have long been overlooked, patients with CF have an unexplained 5-fold increased risk of colorectal cancer. Much of our understanding of the disease has relied on two-dimensional cell lines and animal models. However, the primary changes occurring in human CF epithelial cells remain largely unclear.

Methods: Donor-matched wild-type (WT) and CFTR knockout (KO) human intestinal organoid (HIO) lines were employed to dissect epithelial cell-intrinsic responses to CFTR dysfunction. Knockout was confirmed at the molecular level by qPCR and immunostaining, and functionally by the forskolin-induced swelling assay. Bulk RNA sequencing was then performed to assess key transcriptional differences between WT and KO organoids under steady state conditions and after IFNγ stimulation, and to evaluate the therapeutic potential of calcium channel blockade. Relevant changes were functionally validated using organoid-derived monolayers.

Results: Loss of CFTR expression alone was sufficient to induce profound changes in gene expression across all conditions. Notably, CFTR KO organoids showed higher baseline MUC2 expression and increased THBS2 in an inflamed context. Calcium channel blockade with verapamil reversed these disease-associated changes at the RNA and protein levels.

Conclusions: By utilising gene-edited HIOs derived from the same donor, we reveal epithelial cell-intrinsic mechanisms downstream of CFTR loss. These findings, enabled by our experimental approach, offer important insights into the role of the intestinal epithelium in CF, independent of immune cells, the microbiome, and inflammation. They also lend support for therapeutic targeting of calcium signalling to reverse disease-associated transcriptomic changes.

1. Background

Advances in nutrition and access to CFTR modulators have transformed cystic fibrosis (CF) into a chronic condition. With improved survival, gastrointestinal symptoms have become more common, affecting up to 90% of patients [1]. In particular, chronic, low-grade intestinal inflammation has been increasingly recognised as a hallmark of CF [2]. Moreover, CF patients have an unexplained 5-fold increased risk of colorectal cancer (CRC) [3]. Nevertheless, the epithelial cell-intrinsic mechanisms–defined as those that occur specifically in

Abbreviations: WT, Wild-type; KO, Knockout; HIO, Human intestinal organoid; IEO, Intestinal epithelial organoid; CF, Cystic fibrosis; FIS, Forskolin-induced swelling; CRC, Colorectal cancer; SC, Sigmoid colon; DEG, Differentially expressed gene; hDEG, Highly differentially expressed gene; GSEA, Gene-set enrichment analysis; TA, Transit-amplifying; VER, Verapamil; ROS, Reactive oxygen species; TEER, Transepithelial electrical resistance; EMT, Epithelial-to-mesenchymal transition; ROI, Region of interest.

* Corresponding author.
E-mail address: mz304@cam.ac.uk (M. Zilbauer).
[1] These authors contributed equally to this work.

https://doi.org/10.1016/j.jcf.2026.06.007
Received 8 March 2026; Received in revised form 25 May 2026; Accepted 17 June 2026

intestinal epithelial cells in the absence of the gut microenvironment–that drive CF-related inflammation remain poorly defined.

Two-dimensional cell lines and animal models have shown that CFTR dysfunction can elevate intracellular calcium (Ca^{2+}) signalling [4] and activate downstream pro-inflammatory pathways, namely via changes in store-operated calcium entry (SOCE) and sarcoplasmic/endoplasmic reticulum calcium entry (SERCA) [5]. In contrast, a recent study using *Cftr*-depleted zebrafish models reported a role for voltage-gated calcium channels (VGCCs) in CF-associated Ca^{2+} signalling; typically, VGCCs are described in the context of excitable cell types, such as neurons. In addition, specific blockade of these channels was protective against neutrophilic inflammation and promoted recovery after injury [6]. Nevertheless, we still lack an in-depth exploration of VGCCs in the human CF intestinal epithelium.

In recent years, human intestinal organoids (HIOs) have enabled the study of mechanisms that are otherwise poorly captured by traditional models [7]. Notably, these adult stem cell-derived models retain the structure, function, and polarity of the intestinal epithelium, as well as tissue- and patient-specific features. They also facilitate direct investigation of epithelial cell function in health and disease, free of confounding factors, such as immune cells and the microbiome, making them ideal models for examining the intestinal epithelium in CF. As an example, Dekkers et al. developed the forskolin-induced swelling assay to measure CFTR activity in CF-derived organoids [8]. Using this approach, researchers identified differential treatment responses and phenotypes in patients, highlighting the clinical utility of HIOs [9,10].

Subsequently, we generated CRISPR-edited CFTR knockout (KO) organoids from healthy human sigmoid colon to directly compare them with wild-type (WT) organoids from the same genetic background. This enabled interrogation of CFTR dysfunction in the human intestinal epithelium without confounding factors, such as inter-patient variability or contaminating cell types. In particular, we sought to identify primary changes in the intestinal epithelium–referred to as epithelial cell-intrinsic mechanisms–that contribute to CF-related pathology and colorectal cancer progression. In parallel, we assessed, for the first time in human CF models, the potential of verapamil, a VGCC blocker, to attenuate disease-associated signatures in non-excitable intestinal epithelial cells.

2. Results

2.1. Generating a human intestinal organoid model of cystic fibrosis

First, genome editing was performed using an established CRISPR-Cas9 RNP-based electroporation protocol [11], generating WT and CFTR KO organoid lines from healthy sigmoid colon (SC) HIOs of the same genetic background, confirmed using ICE analysis of Sanger sequencing data. The organoids were then expanded and frozen to generate stocks for downstream experiments.

Upon thawing, the knockout was further validated by qPCR (Fig. 1A) and immunofluorescent staining (Fig. 1B-C), which showed reduced CFTR mRNA and apical protein levels in the KO. We also confirmed loss of CFTR function using the forskolin-induced swelling assay, where KO organoids showed significantly reduced swelling after 24 h of forskolin treatment (Fig. 1D-E). Interestingly, KO HIOs demonstrated reduced growth in 3D Matrigel culture compared with WT HIOs (Fig. 1F).

2.2. Transcriptomic analysis of WT and CFTR KO organoids

Next, we sought to dissect intestinal epithelial cell-intrinsic

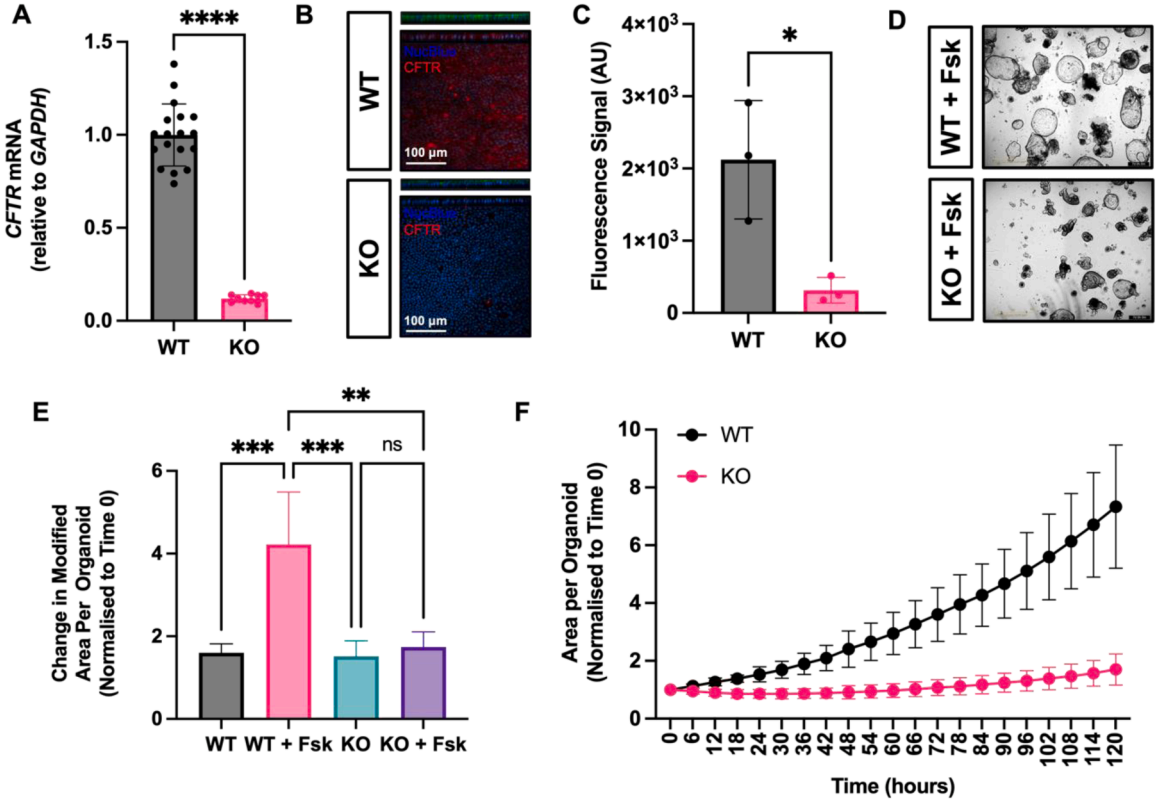

Fig. 1. Molecular and functional validation of CFTR knockout HIOs. (A) qPCR validation of WT/KO CFTR expression. N_{WT}=18, N_{KO}=9, significance by Welch's *t*-test. (B) Representative image and orthogonal view of CFTR staining. The upper panel shows representative apical staining of ActinGreen. Scale bar, 100 µm. (C) Analysis of CFTR immunostaining. N = 3, significance by Welch's *t*-test. (D-E) Representative images (D) and analysis (E) of forskolin-induced swelling of WT/KO organoid lines. N ≥ 3 per condition; significance by one-way ANOVA. (F) Growth of WT/KO organoids over 5 days, normalised to day 0 area. All error bars indicate ±SD.

mechanisms underlying CFTR dysfunction at steady state and under inflammation. For the latter, WT and CFTR KO organoids were exposed to 20 ng/mL IFNγ from day 4 onward, given the documented roles of IFNγ in calcium signalling, cystic fibrosis, and cancer [12–16]. Then, HIOs were submitted for bulk RNA sequencing.

To begin with, the CFTR KO was maintained in culture (Fig. 2A), and unsupervised principal component analysis (PCA) revealed that samples clustered primarily dependent on IFNγ treatment (Fig. 2B).

Differentially expressed gene (DEG) analysis between WT and KO HIOs at steady state and during inflammation revealed profound differences in gene expression (Fig. 2C-D). Moreover, IFNγ induced both shared and unique hDEGs, suggesting differential responses to stimulation driven solely by CFTR dysfunction (Fig. 2E). In particular, only 42% of up-regulated and 9% of down-regulated hDEGs overlapped between donor- and passage-matched WT and CFTR KO HIOs after IFNγ stimulation.

In accordance with mechanisms identified in *Cftr*-depleted zebrafish [6], we confirmed altered expression of gene-sets defining Ca^{2+} transport via voltage-gated calcium channels (GO:0055074) and H_2O_2 metabolic pathways (GO:0042743) in human CFTR KO HIOs at steady state (Fig. 2F-G).

Next, we conducted cell-type deconvolution to assess whether the observed gene expression differences could arise from changes in cell proportions. This approach revealed minor increases in colonocytes and stem cells and decreases in transit-amplifying (TA), goblet, and L cells in KO organoids (Supplementary Fig 2). We found no significant change in the composition of other cell types.

Taken together, these findings indicate that CFTR knockout drastically alters epithelial cell behaviour at steady state and in response to IFNγ stimulation, in the absence of the intestinal microenvironment.

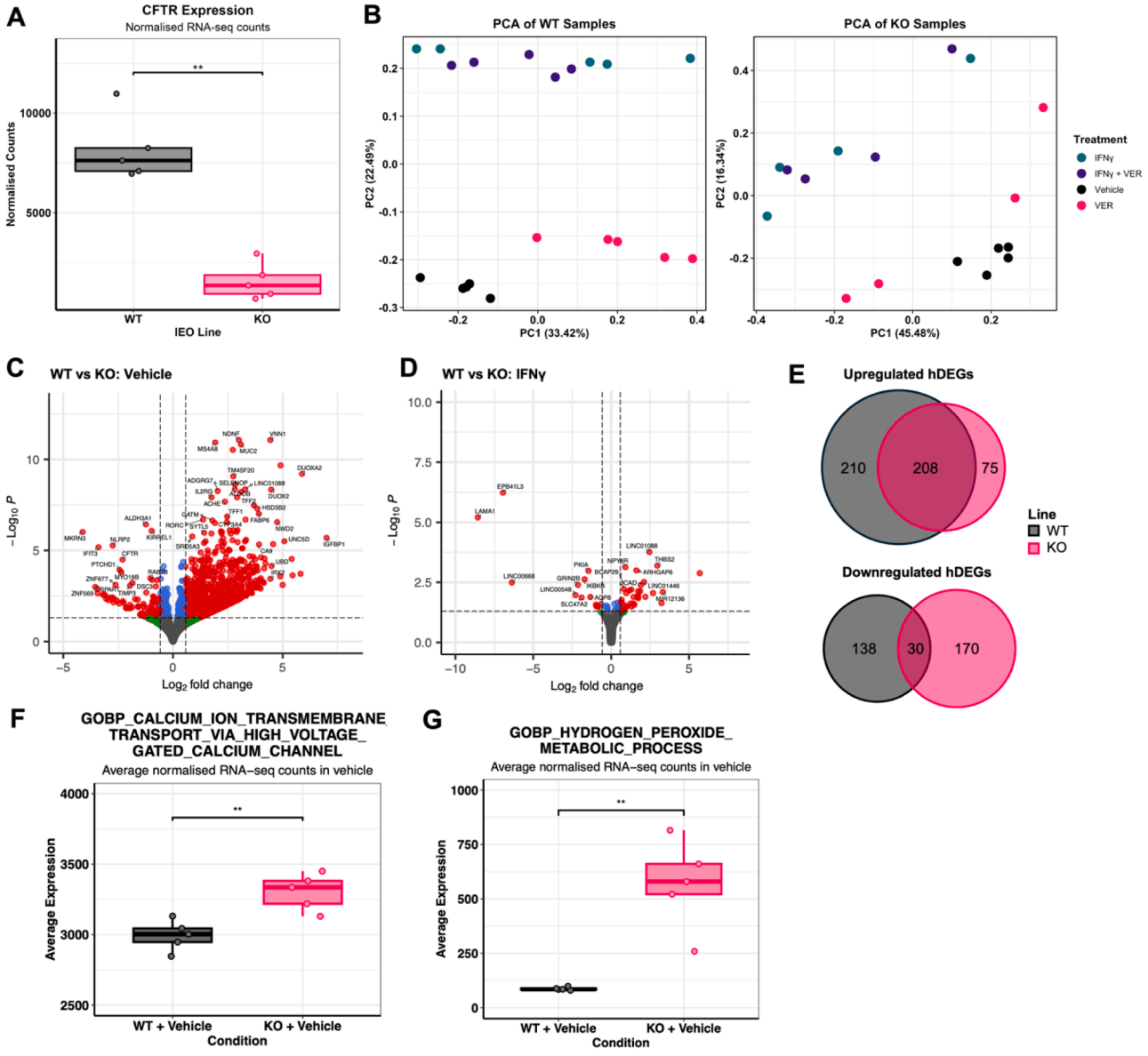

Fig. 2. Bulk-RNA-sequencing analysis of HIOs reveals transcriptomic rewiring downstream of CFTR dysfunction. (A) Normalised CFTR counts in vehicle-treated HIOs. N = 5, significance by Wilcoxon signed-rank test (BH adjustment). (B) PCA plots of bulk RNA sequencing data. (C, D) Volcano plots comparing WT/KO organoids at steady state (C) and after 48 h IFNγ treatment (20 ng/mL). DENN5B-AS1 outside the range in (D). (E) Highly differentially expressed genes (hDEGs: p-adj<0.05, logFC>1) comparing vehicle- and IFNγ-treated organoids. (F, G) Average gene-set expression (F: GO:0055,074; G: GO:0042,743) across conditions. N = 5; significance by Wilcoxon signed-rank test (BH adjustment). All error bars indicate ±SD.

2.3. Calcium channel blockade rescued CF-related gene expression changes

Our previous results reiterate reports that aberrant calcium signalling, namely via VGCCs, arises from abnormal CFTR function [6]. Therefore, we treated organoids with 20 μM verapamil from day 5 (Supplementary Fig 3, 4A) to investigate whether the specific blockade of L-type VGCCs could rescue the observed transcriptional changes.

First of all, no hDEGs between vehicle- and verapamil-treated HIOs were shared between WT and KO organoids, implying differential responses to VGCC inhibition (Fig. 3A-B). Gene-set enrichment analysis (GSEA) revealed that steady state KO organoids were negatively enriched for key biological processes, including the ribosome (hsa03010) and spliceosome (hsa03040), and positively enriched for metabolic processes (Fig. 3C-D). In contrast, verapamil reversed these transcriptomic differences and induced positive enrichment of these pathways in KO HIOs.

Moreover, we confirmed previous findings of increased MUC2 mRNA and protein expression at baseline in human CFTR KO organoids, which reverted toward WT levels after verapamil treatment (Fig. 3E-H). Interestingly, under inflammatory conditions, both WT and KO HIOs showed elevated MUC2 expression, with no verapamil-induced protective effect amid IFNγ stimulation.

We also identified several genes whose expression in CFTR KO organoids diverged from WT levels upon IFNγ treatment, including thrombospondin-2 (THBS2). Notably, verapamil was protective against these IFNγ-induced changes (Fig. 3I).

2.4. Functional validation of verapamil-induced protection against CF-related phenotypes

To confirm the observed differences in growth, mRNA expression levels, and the protective effect of verapamil, we generated HIO-derived monolayers and assessed barrier integrity, cell proliferation, ROS

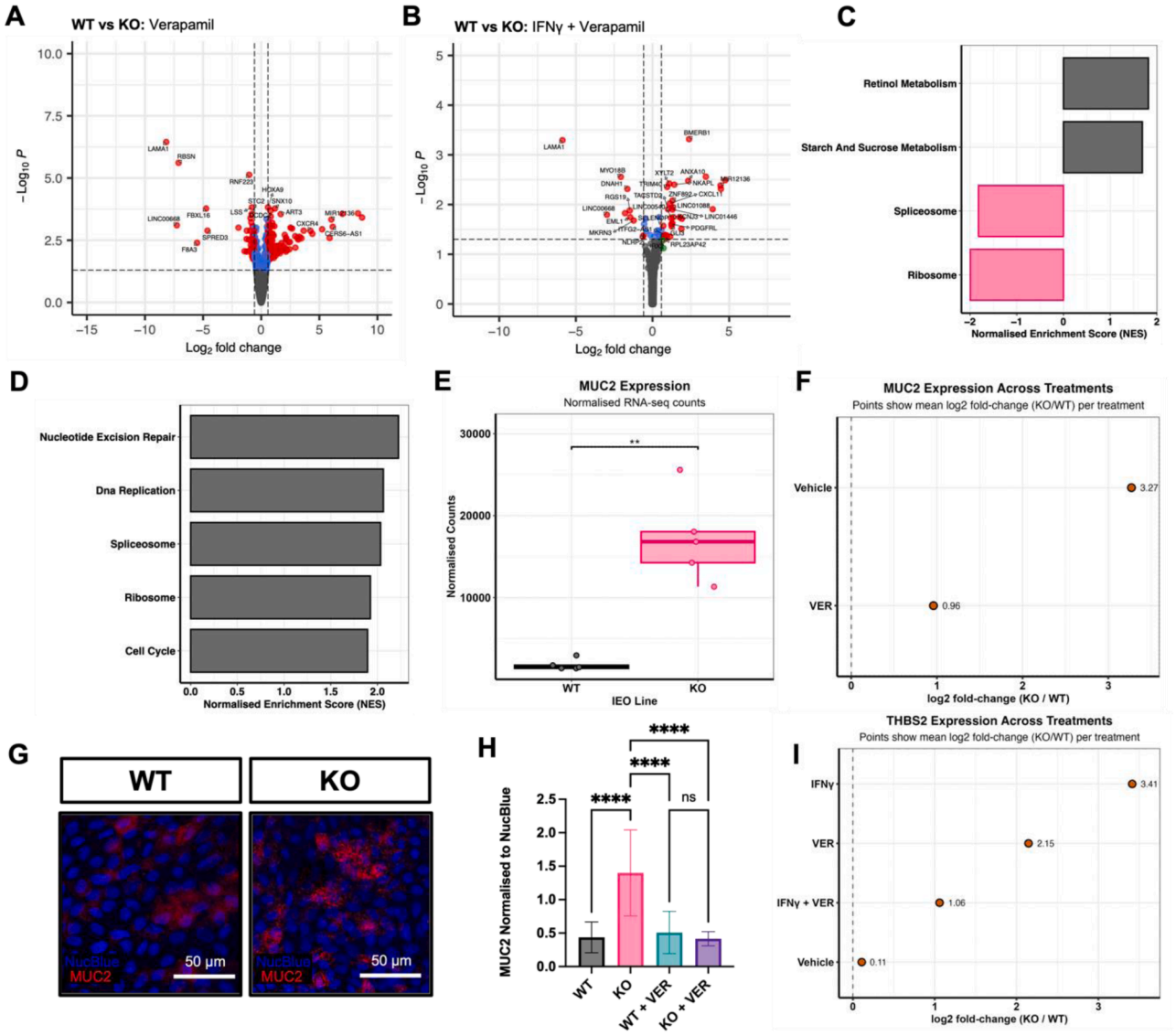

Fig. 3. Verapamil is protective in CFTR KO organoid lines at an RNA and protein level. (A, B) Volcano plots of DEGs between WT/KO organoids after verapamil treatment under steady state(A)/inflammatory(B) conditions. RSC1A1 and PEDS1-UBE2V1 (A) and GABRB3 and PEDS1-UBE2V1 (B) fall outside the axis range. (C) Top KEGG pathways enriched via GSEA for WT versus KO organoids in the vehicle. (D) Top GSEA-enriched KEGG pathways for WT versus KO organoids after verapamil treatment. (E) Normalised counts of WT/KO MUC2 in the vehicle. N = 5; significance by Wilcoxon signed-rank test (BH adjustment). (F) Mean fold-change in WT/KO MUC2 expression. (G-H) Representative panel (G) and quantification (H) of MUC2 in HIOs. N ≥ 2 per condition with N ≥ 6 representative fields. Significance by one-way ANOVA followed by Tukey's multiple-comparisons test. Scale bar, 50 μm (I) Mean fold-change in THBS2 expression comparing KO to WT across treatments. All error bars indicate ±SD.

production, Ca^{2+} responses, and secretion of inflammatory factors.

Notably, we observed no significant difference in proliferation coverage or barrier integrity (TEER) of organoid-derived monolayers across growth and even after treatment (Fig. 4A-B).

We then performed the Fluo4-NW assay to quantify differences in intracellular Ca^{2+}levels after treatment with IFNγ and verapamil. In this context, we observed comparable baseline WT/KO Ca^{2+} levels, with a significant increase in WT monolayers under IFNγ treatment that was rescued by verapamil (Fig. 4C).

We also assessed real-time changes in intracellular Ca^{2+}flux following ATP stimulation, revealing that CFTR KO monolayers showed a significantly elevated and prolonged Ca^{2+} response to ATP under steady state conditions, compared to WT monolayers (Fig. 4D-E). In contrast, IFNγ-treated monolayers, with or without verapamil, demonstrated minimal response to ATP (Fig. 4D-E).

Finally, to examine downstream inflammatory pathways modulated by Ca^{2+}, we sought to validate the THBS2 mRNA rescue by verapamil using an ELISA for basal media supernatants (Fig. 3I). Both WT and KO monolayers peaked in THBS2 secretion early after epithelial differentiation, although KO monolayers secreted significantly higher THBS2 up to day 4 (Fig. 4F). At 100% confluency and after treatment, WT and KO monolayers showed no difference in baseline THBS2 secretion, though IFNγ stimulation increased the THBS2 response in KO monolayers, an effect rescued by verapamil treatment (Fig. 4G-H).

3. Discussion

In this study, we provide evidence that gene-edited, donor-matched HIOs are valuable models for studying epithelial cell-specific changes after CFTR knockout that may contribute to the gastrointestinal manifestations of cystic fibrosis and the progression to colorectal cancer.

In particular, we showed that KO HIOs expand more slowly in 3D Matrigel (Fig. 1F) but display comparable proliferation and TEER in 2D monolayers (Fig. 4A-B). To date, evidence on the effect of CFTR dysfunction on cellular proliferation is conflicting: some studies associated dysfunction with increased cellular proliferation, while others found no difference [17–19]. In our model, we hypothesise that an elevated stem cell and reduced transit-amplifying (TA) cell population could reflect impaired differentiation in KO organoids at baseline, with slower 3D proliferation of these intermediate cells (Supplementary Fig 2). This effect disappears in 2D culture, as the stiff PET transwell surface may trigger mechanosensation-induced proliferation, as in repair and injury pathways [20]. We also observed a shift in differentiation away from the secretory lineage, which may reflect disrupted differentiation in CFTR KO organoids, compromising the balance between stem cell maintenance, expansion, and differentiation. However, bulk cell deconvolution indirectly infers cellular composition and should be validated through single cell RNA sequencing.

Consistent with previous work, this KO model recapitulates CF-

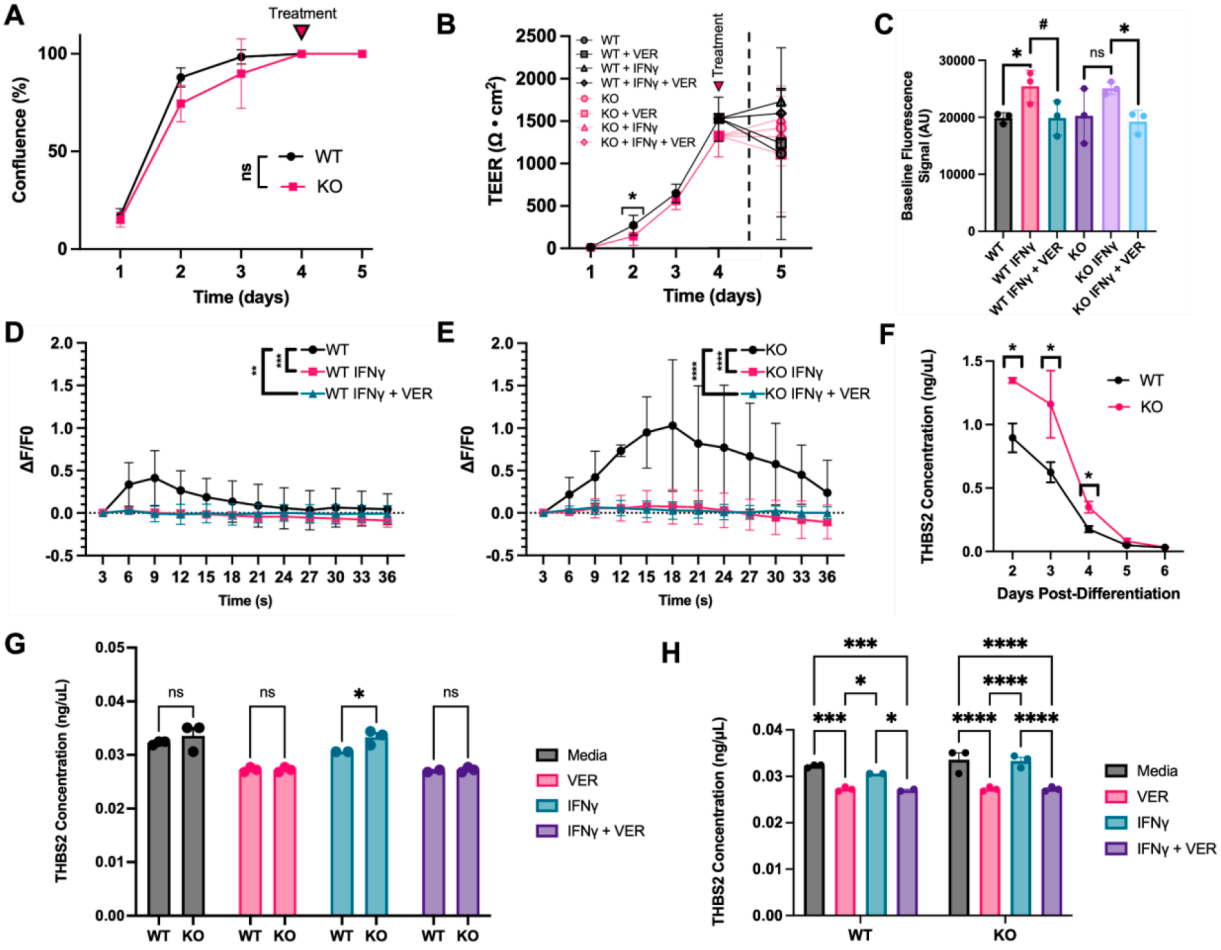

Fig. 4. HIO-derived monolayers to study CFTR dysfunction in the intestinal epithelium. (A) HIO-derived monolayer confluence post-differentiation. N = 18; significance by two-way ANOVA. (B) Daily monolayer TEER measurements after addition of differentiation medium. N = 3, significance by two-way ANOVA. (C) Baseline intracellular Ca^{2+}staining. N = 3; significance by repeated-measures one-way ANOVA. (D, E) Intracellular Ca^{2+} staining of WT (D) and KO (E) organoids after stimulation with 10 μM ATP. N = 3; significance by repeated one-way measures ANOVA. (F) Basal THBS2 concentration at steady state. N = 3; significance by multiple *t*-tests with *post-hoc* BH correction. (G, H) Basal THBS2 concentration at day 6 after IFNγ and verapamil treatment. N ≥ 2; significance by two-way ANOVA. All error bars indicate ±SD.

associated Ca^{2+} signalling dynamics observed in airway epithelial cells and zebrafish models, including an unchanged Ca^{2+} baseline [21] (Fig. 4C) and a hypersensitive Ca^{2+} response [6,22], suggesting that similar mechanisms are at play in the human intestine (Fig. 4D-E). Importantly, the increased expression of Ca^{2+} signalling-related gene sets may prime CF epithelial cells for rapid induction and sustained intracellular Ca^{2+}signalling upon exposure to agonists (Fig. 2F).

We also confirmed that IFNγ increases basal intracellular Ca^{2+}, although this effect was not significant in KO HIOs, potentially due to suppression of the induced Ca^{2+} response or technical fluorophore saturation [22]. Furthermore, intracellular Ca^{2+} levels were comparable between untreated and verapamil plus IFNγ-treated monolayers (Fig. 4C), suggesting that the absent ATP response in monolayers reflects a genuine verapamil-induced decrease (Fig. 4D). Under these circumstances, Ca^{2+} levels were quantified after treatment rather than measured in real time. Future work will benefit from more in-depth analysis of cellular Ca^{2+} signalling dynamics, including integration with alternative mechanisms of entry and export, such as SERCA and SOCE.

Despite this, we could not recapitulate the changes in reactive oxygen species generation observed in *Cftr*-depleted zebrafish, highlighting the complexity of modelling such phenomena (Fig. 2G, Supplementary Fig 6).

We also revealed broad transcriptional remodelling in the KO intestinal epithelium at steady state and during inflammation, including Ca^{2+}-associated changes that were reversed by verapamil. For instance, CFTR KO organoids were negatively enriched for RNA processing and protein synthesis pathways at steady state, suggesting drastic changes in cellular behaviour upon loss of CFTR; a change that was reversed upon treatment with verapamil (Fig. 3C-D)

In addition, mRNA levels and basal secretion of THBS2 were higher in IFNγ-treated KO organoids and monolayers, respectively, and both were dampened by verapamil (Fig. 3I,4F-H). In healthy tissue, THBS2 is involved in remodelling, angiogenesis, and collagen organisation [23–25]. Interestingly, THBS2 was previously identified as differentially expressed in a CFTR KO rat model [26], further supporting the direct physiological relevance of THBS2 downstream of CFTR dysfunction, as observed during early differentiation (Fig. 4F). In disease, increased expression of THBS2 has been associated with elevated inflammatory secretomes [27,28] and fibrosis, providing a potential mechanism for the chronic, low-grade inflammation observed in the CF gut. Moreover, various studies have implicated elevated THBS2 in the progression and prognosis of colorectal cancer through contributing to immune cell infiltration [29] and epithelial-to-mesenchymal transition (EMT) [30–33]. Overall, our data support increased THBS2 expression under non-inflammatory repair conditions and highlight THBS2 as a potential therapeutic target. In the future, clinical follow-up of THBS2 neutralisation may provide further insight.

Finally, studies using mouse models have reported increased MUC2 expression and goblet cell numbers in the CF intestinal epithelium [34–36]. We confirm that MUC2 expression is higher in CFTR KO HIOs, but we observed increased goblet cell populations in CFTR WT organoids from bulk cell deconvolution of the transcriptomic data and no difference from immunofluorescent staining of NucBlue+MUC2+ cells (Fig. 3G-H, Supplementary Fig 2, Supplementary Fig 5), suggesting overproduction of MUC2 rather than an increase in the number of MUC2+ goblet cells. Single-cell RNA sequencing could further address this. We also observed a passage effect on MUC2 expression after extended culture beyond the transcriptomics analysis (Supplementary Fig 4B).

Through this research, we demonstrate several advantages of gene-edited human organoids, including ease of gene editing, scalability, and direct relevance to the human intestinal epithelium. While CF patient-derived IEOs provide a highly accurate model for personalised drug screening [9–10], large sample sizes are required to overcome inter-patient variability. Therefore, using passage-stable CRISPR-edited organoids from the same genetic background eliminates interpatient variability and the need for large-scale transcriptomics to identify pathways affected solely by epithelial cell-specific loss of CFTR.

There is considerable scope for future research to refine and develop organoid culture techniques, including the identification of disease- and tissue-relevant cytokine cocktails that better capture the *in vivo* milieu. Moreover, developing co-culture systems that include immune cells and microbes relevant to CF-related pathology, including neutrophils, will provide greater insight into how CFTR dysregulation directly affects epithelial cell crosstalk and contributes to tumour development. Finally, more extensive comparisons between donor-matched primary tissue and patient-derived organoids, potentially using spatial transcriptomics, will inform CF-relevant disease modules and identify patient-specific sensitivities to verapamil modulation–though access to large patient cohorts will be necessary.

Taken together, by implementing CRISPR-edited human gut organoids, we provide evidence for the importance of VGCCs and Ca^{2+} effector mechanisms in non-excitable intestinal epithelial cells in cystic fibrosis. We also show that treatment with commercially available calcium channel blockers, such as verapamil, could mitigate key disease-associated phenotypes, including elevated MUC2 and THBS2 levels in the CFTR KO epithelium, which may inform future clinical strategies.

4. Methods

4.1. Patient recruitment and sample collection

Forceps biopsies were obtained from the sigmoid colon of children undergoing diagnostic endoscopies at Addenbrooke's Hospital, Cambridge, with full ethical approval (REC-12/EE/0482). Children with macroscopically and histologically normal mucosa were selected as healthy controls.

4.2. Human intestinal organoid culture

Human intestinal organoids (HIOs) were generated from fresh mucosal biopsies and cultured according to published protocols [37,38]. Briefly, crypts were released using 2.5 mM EDTA in PBS and mechanical disruption, before seeding in Matrigel (Corning) domes. Crypts were supplemented with complete medium, followed by media changes every 2 days.

4.3. Monolayer generation

Day 4 organoids were dissociated in pre-warmed TrypLE (Gibco) and seeded at 300,000 single cells per Matrigel-coated transwell (2% v/v in PBS, 1-hour pre-incubation). Monolayers were fed daily with 3DWR0.5 medium. Conditioned medium was harvested from apical and basolateral compartments and stored at −80 °C. TEER measurements were performed (EVOM), and images were captured on the EVOS M3500 daily.

4.4. CRISPR-Cas9 RNP electroporation of HIOs

Knockout organoids were generated according to published protocols using a guide targeting exon 8 of CIITA [11]. In summary, day 5 organoids were dissociated into single cells, resuspended in P3 reaction buffer (Lonza), and incubated with ribonucleoproteins composed of TrueCut Cas9 (Invitrogen) and guide RNA, for 10 min. Then, electroporation was performed according to the manufacturer's instructions (Lonza Amaxa). The cells were collected, re-suspended in Matrigel, and cultured as before. Passage and donor-matched non-edited organoids served as controls. Knockout efficiency was confirmed by ICE analysis of Sanger sequencing data (Synthego). Then, passage-matched WT and CFTR KO HIOs were expanded and frozen in freezing medium

(Sigma-Aldrich) for downstream experiments.

Target	Sequence
CFTR Exon 8 guide RNA	ATACCATGTTTGTACAGCCC
CFTR Fwd	GGCCCAGAGAGATTAAATAACATGCCCA
CFTR Rvs	TCCATCATACTGTCCAGAGAAATGCT

4.5. Co-culture with pro-inflammatory cytokines and calcium channel blockers

HIOs were treated with 20 ng/mL IFNγ (Life Technologies) from day 4, followed by 20 μM verapamil (Merck) in 0.4% DMSO for the final 48 h. HIO-derived monolayers were treated with IFNγ from confluency for 8 h, then with verapamil for the following 16 h at the specified concentrations.

4.6. HIO growth and barrier integrity assessment

Organoids were imaged at 6 hour intervals using the Incucyte SX5 Live-Cell Analysis System (Sartorius). Organoid area, count, darkness, and eccentricity were extracted and analysed using an established pipeline [39].

For the forskolin-induced swelling assay, organoids were treated with 5 μM/L forskolin on day 5 and imaged at 4 hour intervals. Swelling was quantified as above. Wells where the organoid area decreased after a media change due to loss of Matrigel were excluded.

4.7. Measuring intracellular Ca^{2+} and reactive oxygen species in monolayers

Following 24 h of co-culture, as outlined in 4.5, monolayers were assayed using the Fluo4-NW Calcium Assay kit (Invitrogen) to measure intracellular Ca^{2+} after treatment with IFNγ and/or verapamil.

Then, the same monolayers were stimulated apically with 1 μM ATP (Promega) and live-imaged (EVOS M5000, 20x, 1 image/3 s). Downstream analysis was performed on the in-focus planes of the monolayer using FIJI. The calcium response is reported as $\Delta F/F_0$ (change in fluorescence/baseline fluorescence), providing insight into calcium dynamics.

After recovery, monolayers were stained with CellROX Orange to quantify intracellular reactive oxygen species, according to the manufacturer's instructions (Invitrogen), and imaged as above.

4.8. Immunofluorescent staining of HIO-derived monolayers

Monolayers were fixed in 4% PFA (10 min), permeabilised in 0.1% TritonX-100 (10 min), and blocked in 1% BSA in PBS (1-hour). Primary antibodies were incubated overnight at 4 °C: 1:150 MUC2 (ab134119, Abcam); 1:150 CFTR (MA1-935, Invitrogen). Secondary antibodies were incubated for 1-hour at room temperature with NucBlue (Invitrogen): DyLight 488-conjugated anti-mouse IgM (1:500, SA5-10150, Invitrogen); Alexa Fluor 647-conjugated anti-rabbit IgG (1:1000, A-31573, Invitrogen). Monolayers were imaged using the Leica SP8. Organoids were masked, and fluorescence intensities were quantified and normalised to DAPI in FIJI.

For the quantification of MUC2+ cells, an automated macro was generated in Fiji to segment NucBlue+ nuclei and quantify the proportion of MUC2+NucBlue+ regions of interest (ROIs). Nuclei were segmented from the NucBlue channel after conversion to 8-bit, Gaussian blurring with sigma = 1, automatic thresholding using the default light method, mask conversion, and hole filling. Particles were defined as nuclear ROIs with a minimum size of 12 pixels, no upper size limit, and circularity between 0.00 and 1.00. For quality control (QC), composite overlay TIFFs were generated with MUC2 in red, NucBlue in blue, and the nuclear ROI outlined in yellow. The MUC2 signal was quantified as the mean MUC2 intensity within each nuclear ROI. If the mean MUC2 intensity exceeded 12 arbitrary intensity units, the ROI was classified as NucBlue+MUC2+.

4.9. THBS2 enzyme-linked immunosorbent assay

Basal conditioned medium was centrifuged (2000 g, 10 min) to remove cellular debris, diluted 1:2, and assayed using the human THBS2 ELISA kit (ab260051, Abcam) with an extended 3-hour incubation. Endpoint absorbance (OD_{450}) was measured on a microplate reader (SpectraMax) and fitted to a four-parameter curve.

4.10. Harvesting HIOs for RNA extraction

Organoids were harvested and stored in AllProtect tissue reagent (Qiagen) at −80 °C. RNA was extracted using the GenElute Mammalian Total RNA Miniprep Kit (Sigma-Aldrich). Samples for bulk RNA sequencing included an on-column DNase I digestion step (Sigma-Aldrich).

4.11. Gene expression analysis using quantitative PCR

cDNA was prepared using Superscript III Reverse Transcriptase (Invitrogen) for qPCR using Quantifast SYBR Green (Qiagen). The mRNA expression of each gene was normalised to GAPDH and analysed using the ΔΔCt method [40].

Gene	Forward Primer	Reverse Primer
GAPDH	AGGTCGGAGTCAACGGATTT	TGGAAGATGGTGATGGGATT
CFTR	AGTGGAGGAAAGCCTTTGGAGT	ACAGATCTGAGCCCAACCTCA
MUC2	GAGGGCAGAACCCGAAACC	GGCGAAGTTGTAGTCGCAGAG

4.12. Bulk RNA sequencing

Samples were submitted to Cambridge Genomic Services, University of Cambridge, for bulk RNA sequencing. Libraries were single-end sequenced using a P4 50-cycle sequencing kit (Illumina) on a NextSeq 2000 platform (50-base read length, 30–35 M reads per sample).

4.13. Data preprocessing

Pre-processing was completed using nf-core/rnaseq v3.14.0, within Bioconda and Biocontainers projects. The pipeline was run with Nextflow v24.10.4 (GRCh38 reference genome), STAR for alignment, and Salmon for quantification.

4.14. Differential gene expression analysis

Differential gene expression analysis was performed using nf-core/differentialabundance v1.40 and executed with Nextflow v24.10.4. Samples with a median absolute deviation (MAD) >5 and genes with <1 count in >50% of samples were excluded from downstream analysis. Genes with p-adj<0.05 were considered DEGs. Of these, genes with abs (logFC)>1 were considered highly DEGs (hDEGs).

4.15. Sample clustering and gene-set enrichment analysis

The R packages ggbio v1.20.1 and clusterProfiler v4.10.1 were used for principal component analysis and gene-set enrichment analysis of pathways comprising 25–500 genes. Significance was set at p-adj<0.05.

4.16. Statistics and reproducibility

Statistical analyses were performed in GraphPad Prism v10.6.1 or R v4.4.1. Error bars represent mean ±SD, unless indicated otherwise. For

multiple comparisons, the adjusted p-value (Benjamini-Hochberg) was used to control the false discovery rate. Comparisons were non-significant unless stated otherwise. * <0.05, **<0.01, ***<0.001, ****<0.0001.

4.17. Visualisation

The graphical abstract was made in BioRender. Slater, E. (2026) https://biorender.com/z4ky3qm.

Ethics statement

All studies using human tissue were conducted with informed consent from the patient and parent and/or legal guardian and with approval from a local ethics committee (REC-17/EE/0265). All methods were performed in accordance with the relevant guidelines and regulations.

CRediT authorship contribution statement

Ellie Slater: Data curation, Methodology, Investigation, Visualization, Validation, Formal analysis. **Woo Jin Yang:** Methodology, Investigation, Visualization, Formal analysis, Validation. **Nefeli Skoufou-Papoutsaki:** Methodology, Resources, Writing – review & editing. **Stephen A. Renshaw:** Conceptualization, Funding acquisition, Writing – review & editing. **Róisín M. Owens:** Conceptualization, Funding acquisition, Writing – review & editing. **Matthias Zilbauer:** Conceptualization, Funding acquisition, Writing – review & editing.

Declaration of competing interest

We declare no financial or personal interest that could bias this research.

Acknowledgements

ES was funded by the Cystic Fibrosis Trust Strategic Research Centre 018 (G107734). W.J.Y. was supported by a Cytiva-sponsored PhD studentship. N.S.-P was funded by the Wellcome Trust (CRUK, 102160/Z/13/Z). Processing of human tissues and generation of human HIOs was supported by the Helmsley Charitable Trust, funded by The Leona M and Harry B Helmsley Charitable Trust grant (G118500).

Supplementary materials

Supplementary material associated with this article can be found, in the online version, at doi:10.1016/j.jcf.2026.06.007.

Data availability

Data is available upon reasonable request.

References

[1] Anton-Păduraru D-T, et al. Diagnosis and management of gastrointestinal manifestations in children with cystic fibrosis. Diagnostics 2024;14:228.
[2] Werlin SL, et al. Evidence of intestinal inflammation in patients with cystic fibrosis. J Pediatr Gastroenterol Nutr 2010;51:304–8.
[3] Birch RJ, et al. The risk of colorectal cancer in individuals with mutations of the cystic fibrosis transmembrane conductance regulator (CFTR) gene: an English population-based study. J Cyst Fibros 2023;22:499–504.
[4] Martins JR, et al. F508del-CFTR increases intracellular Ca2+ signaling that causes enhanced calcium-dependent Cl− conductance in cystic fibrosis. Biochim Biophys Acta - Mol Basis Dis 2011;1812:1385–92.
[5] Tabary O, et al. High susceptibility for cystic fibrosis Human airway gland cells to produce IL-8 through the iκb kinase α pathway in response to extracellular NaCl content. J Immunol 2000;164:3377–84.
[6] Cornélie S, et al. Verapamil limits inflammation by restoring VGCC-driven epithelial Ca2+ in models of cystic fibrosis. Preprint at bioRxiv 2025. https://www.biorxiv.org/content/10.1101/2025.10.12.681885v1.
[7] Kraiczy J, Zilbauer M. Intestinal epithelial organoids as tools to study epigenetics in gut health and disease. Stem Cells Int 2019;2019:1–7. 2019.
[8] Dekkers JF, et al. A functional CFTR assay using primary cystic fibrosis intestinal organoids. Nat Med 2013;19:939–45.
[9] Boj SF, et al. Forskolin-induced Swelling in Intestinal Organoids: an *In Vitro* Assay for Assessing Drug Response in Cystic Fibrosis Patients. J Vis Exp 2017. https://www.jove.com/t/55159/forskolin-induced-swelling-intestinal-organoids-an-vitro-assay-for.
[10] Ramalho AS, et al. Correction of CFTR function in intestinal organoids to guide treatment of cystic fibrosis. Eur Respir J 2021;57:1902426.
[11] Skoufou-Papoutsaki N. Efficient genetic editing of human intestinal organoids using ribonucleoprotein-based CRISPR. Dis Model Mech 2023;16.
[12] Iwagaki H, Fuchimoto S, Miyake M, Aoki H, Orita K. Interferon-gamma activates the voltage-gated calcium channel in RPMI 4788 cells. Biochem Biophys Res Commun 1988;153:1276–81.
[13] Aas V, Larsen K, Iversen J-G. Interferon-γ elicits a G-protein-dependent Ca2+ signal in Human neutrophils after depletion of intracellular Ca2+ stores. Cell Signal 1999;11:101–10.
[14] Raia V, et al. Evidence of chronic inflammation in morphologically normal small intestine of cystic fibrosis patients. Pediatr Res 2000;47:344–50.
[15] Wrigley-Carr HE, van Dorst JM, Ooi CY. Intestinal dysbiosis and inflammation in cystic fibrosis impacts gut and multi-organ axes. Med Microecol 2022;13:100057.
[16] Monteith GR, Prevarskaya N, Roberts-Thomson SJ. The calcium–cancer signalling nexus. Nat Rev Cancer 2017;17:373–80.
[17] Liu K, et al. Defective CFTR promotes intestinal proliferation via inhibition of the hedgehog pathway during cystic fibrosis. Cancer Lett 2019;446:15–24.
[18] Verstegen MMA, et al. Human extrahepatic and intrahepatic cholangiocyte organoids show region-specific differentiation potential and model cystic fibrosis-related bile duct disease. Sci Rep 2020;10:21900.
[19] Hayes D, et al. Cell Therapy for cystic Fibrosis lung disease: regenerative basal Cell amplification. Stem Cells Transl Med 2019;8:225–35.
[20] Gjorevski N, et al. Designer matrices for intestinal stem cell and organoid culture. NatureNature 2016;539:560–4.
[21] Murphy E, Cheng E, Yankaskas J, Jackson Stutts M, Boucher RC. Cell calcium levels of normal and cystic fibrosis nasal epithelium. Pediatr Res 1988;24:79–84.
[22] Ribeiro CMP, Paradiso AM, Carew MA, Shears SB, Boucher RC. Cystic fibrosis airway epithelial Ca2+ signalling. J Biol Chem 2005;280:10202–9.
[23] Kyriakides TR, et al. Mice that lack thrombospondin 2 display connective tissue abnormalities that are associated with disordered collagen fibrillogenesis, an increased vascular density, and a bleeding diathesis. J Cell Biol 1998;140:419–30.
[24] Tsai EA, et al. THBS2 Is a candidate modifier of liver disease severity in Alagille syndrome. Cell Mol Gastroenterol Hepatol 2016;2:663–675.e2.
[25] Kyriakides TR, Zhu Y-H, Yang Z, Huynh G, Bornstein P. Altered extracellular matrix remodeling and angiogenesis in sponge granulomas of thrombospondin 2-null mice. Am J Pathol 2001;159:1255–62.
[26] de Lisle RC KJ. RNA-seq analysis of the cystic fibrosis rat small intestine. Accessed on 8 Feb, https://www.ncbi.nlm.nih.gov/geo/query/acc.cgi?acc=GSE81114; 2026.
[27] Yu L, et al. Enhanced THBS2 promotes collagen synthesis and inflammatory secretome of fibroblasts in idiopathic pulmonary fibrosis. Sci Rep 2025;15:25926.
[28] Lin J, et al. Identification of the M2 macrophage-associated gene THBS2 as a predictive marker for inflammatory cancer transformation. Inflamm Bowel Dis 2025;31:963–74.
[29] Liao X, Wang W, Yu B, Tan S. Thrombospondin-2 acts as a bridge between tumor extracellular matrix and immune infiltration in pancreatic and stomach adenocarcinomas: an integrative pan-cancer analysis. Cancer Cell Int 2022;22:213.
[30] Qu H, Hasen G, Hou Y, Zhang C. THBS2 promotes cell migration and invasion in colorectal cancer via modulating wnt/β-catenin signaling pathway. Kaohsiung J Med Sci 2022;38:469–78.
[31] Wang X, et al. THBS2 is a potential prognostic biomarker in colorectal cancer. Sci Rep 2016;6:33366.
[32] Huang J, et al. Molecular mechanisms of thrombospondin-2 modulates tumor vasculogenic mimicry by PI3K/AKT/mTOR signaling pathway. Biomed Pharmacother 2023;167:115455.
[33] Zhang C, et al. The integrative analysis of thrombospondin Family genes in Pan-cancer reveals that THBS2 facilitates gastrointestinal cancer metastasis. J Oncol 2021:1–19. 2021.
[34] Malmberg EK, et al. Increased levels of mucins in the cystic fibrosis mouse small intestine, and modulator effects of the Muc1 mucin expression. Am J Physiol Gastrointest Liver Physiol 2006;291:G203–10.
[35] Gustafsson JK, et al. Bicarbonate and functional CFTR channel are required for proper mucin secretion and link cystic fibrosis with its mucus phenotype. J Exp Med 2012;209:1263–72.
[36] Kelly J, et al. Alterations of mucosa-attached microbiome and epithelial cell numbers in the cystic fibrosis small intestine with implications for intestinal disease. Sci Rep 2022;12:6593.
[37] Howell KJ, et al. DNA methylation and transcription patterns in intestinal epithelial cells from pediatric patients with inflammatory bowel diseases differentiate disease subtypes and associate with outcome. Gastroenterology 2018;154:585–98.

[38] Kraiczy J, et al. DNA methylation defines regional identity of human intestinal epithelial organoids and undergoes dynamic changes during development. Gut 2019;68:49–61.

[39] Yang W, Blahusova E, McCoy R, Owens RM, Zilbauer M. Novel quantitative assessment pipeline of organoid growth dynamics using adapted light absorption and surface area normalization models. Adv Nanobiomed Res 2025;5.

[40] Livak KJ, Schmittgen TD. Analysis of relative gene expression data using real-time quantitative PCR and the 2−ΔΔCT method. Methods 2001;25:402–8.